2011 50th IEEE Conference on Decision and Control and
European Control Conference (CDC-ECC)
Orlando, FL, USA, December 12-15, 2011

Design and Implementation of an Atomic Force Microscope with Adaptive Sliding Mode Controller for Large Image Scanning

Yuan-Zhi Peng, Jun-Wei Wu, Kuan-Chia Huang, Jyun-Jhih Chen,
Mei-Yung Chen, and Li-Chen Fu, *Fellow, IEEE*

***Abstract*—Atomic force microscopy (AFM) is an advanced technique which aims to scan a sample through the use of a probe or a tip; however, conventional atomic force microscope system suffers from the limitation of small scanning range, due to the short travelling range of piezoelectric actuation. In this paper, we propose a large measurement- range AFM scanning system which combines both fine positioners of piezoelectric and electromagnetic actuations. While the piezoelectric positioner provides high speed scanning with nanometer resolution, the precision electromagnetic positioner is capable of 1 mm² large field positioning with 30 nm rms error. The overall design of the stage consists of 4 pairs of electromagnetic actuator, monolithic serial flexure guidance with compression springs, an eddy current damper, and a commercial *xyz* piezoelectric positioner. Besides, a stationary compact disk/digital versatile disk pick-up-head (CD/DVD PUH) is used to measure the amplitude of samples. Moreover, an adaptive sliding mode controller based on the analytical modeling is used to overcome the unmodeled system uncertainties and external disturbances. Finally, preliminary experiments are presented, demonstrating feasibility of the proposed system.**

***Index Terms*—Precision motion control, electromagnetic actuation, CD/DVD PUH, adaptive sliding mode control**

I. INTRODUCTION

Since the invention of atomic force microscope (AFM) in 1986 [1], it has been widely used in the field of nanotechnology. Based on the similar principle, many powerful tools were developed, for example, magnetic force microscope [2], friction force microscope [3], and electrostatic force microscope [4], which can be generally named as scanning force microscope, are developed for various applications with different measured forces. The use of AFM [5] enables researchers to observe sample surfaces in nanoscale and results in progressive changes in biology, physics, chemistry, and material science [6].

However, limited to the travelling range of piezoelectric actuators, traditional AFM can hardly scan a sample size over 100 μm. In practice, taking biology for example, biological samples can be as small as tens nanometers, like microtubules ($\approx$25 nm) and ribosomes ($\approx$11 nm), and as large as hundreds of micrometers, like amoeba ($\approx$800 μm) and the ovum of human beings ($\approx$100 μm). Hence, a high-resolution AFM system with millimeter scanning range will contribute a lot to many researches like this.

Nowadays, there are researches around the world focusing on this topic, too. In 2007, Sinno in France proposed the concept of a homemade sample-holder used for nanopositioning with a millimeter traveling range in two dimensions [7]. This sample-holder featured a coarse to fine displacement actuation and was realized in 2009 [8]. In 2009, Eves in Canada proposed the design of a large measurement-volume metrological AFM. The translation of the stage is also accomplished with coarse and fine stages, and the scanning volume is up to 40 mm × 40 mm × 6 mm [9]. In 2010, Werner in Netherland developed a concept of a novel metrological AFM. The instrument consists of a translation stage with a stroke of 1x1x1 mm³, and Lorentz-actuators with weight and stiffness compensation are utilized as its actuation unit [10], but the conceptual stage has not been proved by any practical experiments.

Beyond many choices of long range actuations, positioning stages basing on the electromagnetic actuation are considered to be a good choice when high precision and long travelling range (millimeter level) are needed simultaneously [11]-[15], and this has encouraged us to build some positioning systems upon electromagnetic actuation [16]-[20]. With our homemade precision electromagnetic positioner (PEP), the sample can be positioned in a field of 1 mm² with 30 nm rms error, but to maintain this high precision, the operating frequency is too slow to scan a sample efficiently (according to our previous research, it cannot be greater than 12 Hz [21]). As a result, we utilize the piezoelectric positioner, which is the most widely used actuation in AFM, to achieve sample scanning in micrometer scale with nanometer resolution, and expand the range to millimeter scale with the help of PEP. Differing from the general coarse-to-fine stages, the two stages we use in this research are both fine stages.

Here, in this paper, we will focus on the design, implementation and control of the AFM system. Featured mechanism designs are presented in Section II. And in Section III, the analytical model and dynamic formulation are derived as basis for subsequent controller design. Furthermore, to overcome the external noises and model uncertainties of electromagnetic actuation, an advanced controller, named adaptive sliding mode controller, is developed for precision positioning in Section IV. The preliminary experimental results are presented in Section V, indicating the positioning ability of PEP.

Manuscript received March 15, 2011. This work was supported by the National Science Council, R.O.C. under Grant NSC 97- 2221- E- 002- 178- MY3.

Yuan-Zhi Peng, Jun-Wei Wu, Kuan-Chia Huang, Jyun-Jhih Chen, Li-Chen Fu are with the Electrical Engineering Department, National Taiwan University, Taipei, Taiwan (e-mail: lichen@ntu.edu.tw)

Mei-Yung Chen is with the Mechatronic Technology Department, Nation Taiwan Normal University, Taipei, Taiwan (e-mail: cmy@ntnu.edu.tw)

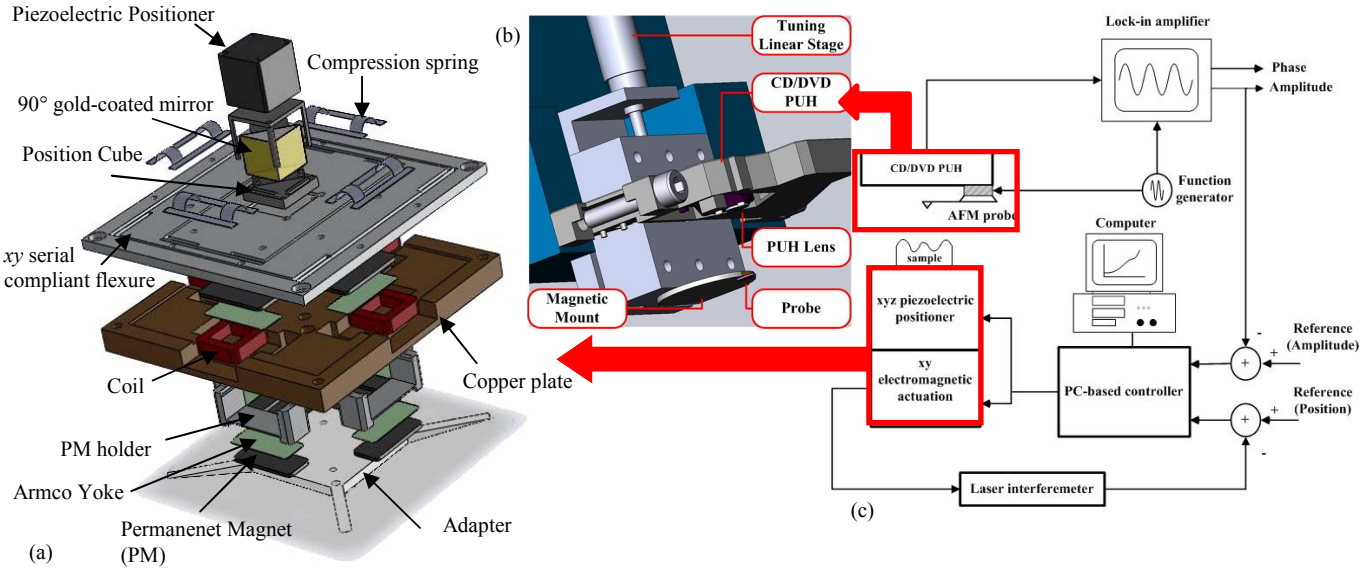

Fig.1 (a) The moving part- explosion view of the PEP with piezoelectric positioner. (b) The stationary part (b) Schematic drawing of the AFM system

II. Mechanism Design

The overall AFM system scheme is shown in Fig. 1 (c). The design of mechanism is mainly divided into the stationary part and the moving part. Samples are placed on the moving part, allowing the probe's position of AFM to remain fixed so that the Abbe errors can be minimized.

The stationary mechanism (see Fig. 1(b)) includes a CD/DVD PUH, a fine tuning linear stage, a bimorph (piezoelectric element), a magnet, and a magnetic mount. The CD/DVD PUH is a detection sensor to measure the oscillation amplitude of the cantilever, whereas the fine tuning linear stage is used to adjust the position of the PUH's laser beam so that it focuses on the cantilever. Moreover, the magnetic mount is used to fix the probe, and the bimorph is employed to oscillate the cantilever of the probe.

The explosion view of PEP with piezoelectric positioner is shown as Fig. 1(a). The overall structure consists of an adaptor fixing the whole stage onto a vibration-isolation optical table. Here, PEP is composed of a monolithic *xy* serial compliant flexure plate with two pairs of compression springs, four pairs of electromagnetic actuator, and one eddy current damper. To measure the position information, a position cube with a 90 degree gold-coated mirror is screw-locked onto PEP as the scanning unit, reflecting the laser beams from laser interferometer. A commercial piezoelectric positioner Piezosystem- Jena Tritor 38, which has the motion range of 38 μm in *xyz* axes with high resolution in nm and sub-nm range, is located at the topmost part. The whole dimensions of PEP are 135 × 135 × 70 mm³. The featured parts of PEP and the sensing system will be detailed in the following subsections.

A. Compliant mechanism with Compression springs

A compliant mechanism transmits motion and forces through deformation of the composing material. Due to the monolithic characteristic, it does not require lubrication unlike rigid body mechanisms. Thus, it has no wear, noise, and backlash. Besides, in the region within its elasticity limits, this mechanism has high repeatability, accuracy, linear force–displacement relation, continuous motion, and is simple to assemble. Over these advantages, compliant mechanisms are well-suited for tasks that require high precision.

In order to attain the large working range up to millimeter level, the leaf-spring type flexure beam is hereby adopted. The monolithic *xy* serial compliant mechanism of flexure beams includes two pairs of leaf springs which are arranged orthogonally and in charge of motions along *x*-, and *y*- direction respectively. To fabricate the designed delicate width (0.3 mm) of the flexure beams, electrical discharging wire cutting (EDWC) was utilized. Moreover, aluminum alloy 7075 with Young's modulus of elasticity E = 72 GPa and density ratio ρ = 2.81 g/cm³, which has a relatively high value of E/ρ, is chosen, because a light and stiff material (low ρ and high E) can ameliorate the band width and the stiffness of the moving stage [22].

To suppress the vibration of flexure mechanisms, two pairs of compression springs made of Al 7075 are implemented along the two axes, as shown. These springs with thickness of 0.3 mm are originally flat and were bended between the fixed and moving parts to generate compression forces. The forces in each pair are equal and opposite in direction, converging to the center of the stage. Therefore, the stage is clipped from both sides, depressing the vibration.

B. Electromagnetic Actuation

Voice coil motor (VCM) is one kind of the linear direct-current motor. It can produce a linear thrust force proportional to the current flowing through the magnetic field. The illustration of VCM and the generated force is shown in Fig. 2. Two NdFeB permanent magnets are placed parallelly above and below the partial side of a rectangular coil by a PM holder (omitted in this figure). With vertically opposite polarity, a near-uniform magnetic field is generated.

Two Armco yoke in between are used as pole shoes that linearize the magnetic field and reduce the nonlinearity problem of electromagnetic actuation as well.

In PEP, four sets of VCM are employed as its electromagnetic actuators. Every pair of VCMs provide the actuation in one axis, and for the purpose of avoiding the lost heat and assembled wires of the coils, all coils are attached on the stationary copper layer whereas the permanent magnets are mounted on the moving *xy*-platen with PM holders, as shown in Fig. 1 (a).

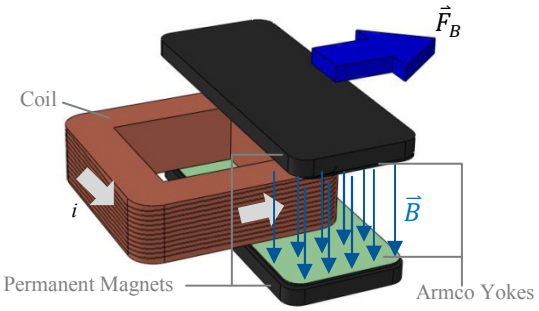

Fig. 2 The illustration of VCM with generated force

C. Eddy Current Damper

Since flexure mechanisms bring about a small damping ratio, a contactless Eddy current damper is designed and used as passive suppression for vibration. When a non-ferromagnetic conductor moves in a magnetic field, or a moving and varying magnetic field intersects a non-ferromagnetic conductor, the relative motion induces a current loop, so called Eddy current, within the conductor. Hence, the generated force can resist the relative motion between the magnetic field and the conductor. This mechanism is compactly designed as the copper plate in Fig. 1 (a), and it produces a very precise damping force without mechanical wear.

D. The Sensing System

A 632 nm He-Ne laser interferometer system featuring nanometer resolution and high sampling rate by Agilent Corp. is employed as the sensor for two-axis measurement for PEP. As the explosion view shown in Fig. 1 (a), a gold-coated right angle specialty mirror with ±2 arcmins angle tolerance is fixed at the center of the positioner. The protected gold is the most efficient reflective coating which allows 96% average reflection. The whole laser beam paths designed in *x*-axis and *y*-axis share equal length and intensity of the laser beam from one laser source.

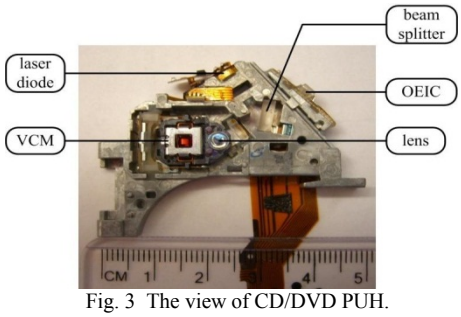

Fig. 3 The view of CD/DVD PUH.

Unlike other traditional AFM sensor, we use a commercial CD/DVD PUH (as shown in Fig. 3) to detect the oscillation amplitude of the probe in the *z*-axis. It has sufficient sensitivity for the application of tapping mode AFM and is a compact and cost-effective detection sensor. Besides, the laser spot of the CD/DVD PUH is smaller than the width of the AFM's cantilever, so the laser energy will not be leaked to the reflective sample to cause sensing errors.

III. Modeling and Dynamic Formulation

A. Electromagnetic Force Analyises

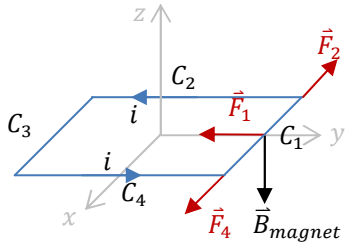

Fig. 4 Electromagnetic force characterization

In the analysis of actuation, the electromagnetic force of this actuator can be analyzed by means of Lorentz Force Principle. From Fig. 4, we can divide one turn coil into four parts, i.e. C_1, C_2, C_3, and C_4, and define $\vec{B}_1$, $\vec{B}_2$, $\vec{B}_3$, and $\vec{B}_4$, as the corresponding magnetic fields generated by the arranged magnets. Since C_3 is not intersected by the magnetic field, $\vec{B}_3$ is assumed to be zero. Besides, the forces $\vec{F}_2$ and $\vec{F}_4$ generated by C_2 and C_4 are equal and opposite in direction, so the total electromagnetic force $\vec{f}_{rec}$ generated by the one-turn coil is

$$\begin{aligned}\vec{f}_{rec} &= \oint_c d\vec{f} = \oint_c id\vec{l} \times \vec{B} \\ &= \int_{c_1} id\vec{l}_1 \times \vec{B}_1 + \int_{c_2} id\vec{l}_2 \times \vec{B}_2 + \int_{c_4} id\vec{l}_4 \times \vec{B}_4 \\ &= [0 \quad iLB \quad 0]^T \end{aligned} \tag{1}$$

where $\vec{B}$ is defined as $\vec{B} \equiv \vec{B}_i = \vec{B}_{magnet}$, $i = 1 \sim 4$.

If the coil has N turns, the lateral force can hence be written as:

$$\vec{F}_{rec} = NLB_{magnet} i = C_{rec} u_{rec} \tag{2}$$

where $\vec{F}_{rec}$ means the total actuated force due to the rectangular coil, L means the edge length of the coil, C_{rec} is defined as the force constant and u_{rec} rather than the variable i is used to denote all the current inputs into rectangular coils.

B. Dynamics Formulation of PEP

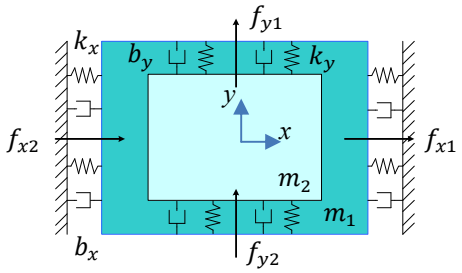

Fig. 5 The dynamic modeling of serial structure

In the dynamics analysis, the serial flexure mechanism can be modeled as a spring–mass-damper system. Due to design of the symmetrical flexure mechanism, we can decouple the dynamics on *x*-axis and *y*-axis. Besides, the hysteresis effect and thermal drift are regarded as the disturbances. From Fig. 5, we define x and y as the displacements along x and y axis, respectively, and through the help of Newton's Law, the system dynamics can be expressed in the following form:

$$(m_1 + m_2)\ddot{x} = F_x - k_x \cdot x - b_x \cdot \dot{x}$$
$$(m_2)\ddot{y} = F_y - k_y \cdot y - b_y \cdot \dot{y} \quad (3)$$

where m_1 is the mass of outer stage allowing the one-DOF constrained motion along *x*-axis only, and m_2 is the mass of the inner stage contributing to *y*-axis motion while moving along *x*-axis with outer stage simultaneously. The notations k_x and k_y are the coefficients of elasticity, b_x and $b_y$are the damping constants, F_x and F_y are the control efforts. Substituting the practical electromagnetic forces analyzed in Eq. (2), we can then rewrite the horizontal actuation and the dynamical equation of the two SISO (Single-input single -output) systems as:

$$(m_1 + m_2)\ddot{x} = -k_x \cdot x - b_x \cdot \dot{x} + 2C_{rec} \cdot u_x$$
$$(m_2)\ddot{y} = -k_y \cdot y - b_y \cdot \dot{y} + 2C_{rec} \cdot u_y \quad (4)$$

To simplify the representation of equation of motion, we define a variable vector as $X = [x \quad y]^T$and reformulate the dynamical equations as:

$$M\ddot{X} = KX + B\dot{X} + CU \quad (5)$$

where M is the inertia term, K is the restoration term,B is the damping term, G is the gravity term,C is force-current factor, and U is the control effort, and related parameters can be defined as:

$$M = \begin{bmatrix} m_1 + m_2 & 0 \\ 0 & m_2 \end{bmatrix}, \quad K = \begin{bmatrix} -k_1 & 0 \\ 0 & -k_2 \end{bmatrix},$$
$$B = \begin{bmatrix} -b_1 & 0 \\ 0 & -b_2 \end{bmatrix}, C = \begin{bmatrix} 2C_{rec} & 0 \\ 0 & 2C_{rec} \end{bmatrix}, U = \begin{bmatrix} u_x & 0 \\ 0 & u_y \end{bmatrix} \quad (6)$$

IV. Controller Design

In order to establish the capability of online gain-tuning as well as the robustness, in this research work, the adaptive law and a sliding mode controller are integrated as a nonlinear control. First, to design a robust controller, the model uncertainty, external noise and disturbance should be taken into consideration in the dynamics modeling. Thus, Eq. (5) is rewritten as:

$$\ddot{X} = M^{-1}KX + M^{-1}B\dot{X} + M^{-1}CU + W_c + W_v \quad (9)$$

where additional uncertainties, including constant uncertainty W_c denoted as the model uncertainty and varying uncertainty W_v denoted as the external noise and disturbances, are added. Assume the varying uncertainty is bounded with $\|W_v\| \le \overline{W}$.

Then, we define the desired position vector as X_d, and the error between the desired vector $X_d$and the position X can be expressed as:

$$E = X - X_d = [x - x_d \quad y - y_d]^T \quad (10)$$

Substituting Eq. (9) into Eq. (10), the reformulated dynamic term can be written as:

$$\ddot{E} = M^{-1}KX + M^{-1}B\dot{X} + M^{-1}CU + W_c + W_v + W_S - \ddot{X}_d \quad (11)$$

Therefore, this plant is processed as one MIMO system; in this way, the inevitable coupling between *x*- and *y*- axis are taken into account, and can be treated as the coupling terms in the coefficient matrices estimated by the adaptive law. To simplify the notations, we define $M^{-1}K$ as K_0, $M^{-1}B$ as B_0, and $M^{-1}C$ as C_0, so that Eq. (11) can be re-expressed as:

$$\ddot{E} = K_0X + B_0\dot{X} + C_0U + W_c + W_v + W_S - \ddot{X}_d \quad (12)$$

A. Adaptive Sliding Mode Controller

Assume the sliding surface S, with the following form:

$$S = \dot{E} + \lambda E \quad (13)$$

where $\lambda = diag[\lambda_1 \quad \lambda_2]$ is a designed positive diagonal matrix. From Eq. (13), we can easily find that the sliding surface is a function consisting of the error term and its time derivative. Generally, our main purpose is to drive the sliding surface to zero, which simultaneously drives E and $\dot{E}$ to zero as well. If the sliding surface tends to be zero within finite time, then E and $\dot{E}$also converge to zero exponentially.

Consequently, the adaptive sliding mode controller is enforced online estimating system parameters and synthesizing the necessary state feedback while simultaneously tuning the controller gains to satisfy the control objective [24]. Based on the sliding surface dynamics, the control law is designed as:

$$U = \hat{C}_0^{-1}(\ddot{X}_d - \hat{K}_0X - \hat{B}_0\dot{X} - \hat{W}_c - QS - Nsgn(S) - \lambda\dot{E}) \quad (14)$$

where $\hat{C}_0$, $\hat{K}_0$, $\hat{B}_0$, and $\hat{W}_c$ are the estimated value of C_0, K_0, B_0 , and W_c , respectively; $Q \equiv diag[q_1 \quad q_2], \forall q_i > 0$; $N \equiv diag[\eta_1 \quad \eta_2], \forall \eta_i > 0$ is the high gain used to bound the variable uncertainty W_v, namely, $\|\eta_i\| \le \overline{W}$; *sat*(.) is the saturation function defined as

$$sat(S) \equiv \begin{cases} 1 & ,S > \varepsilon \\ \frac{S}{|\varepsilon|} \quad if & ,-\varepsilon \le S \le \varepsilon, \forall \varepsilon > 0 \\ -1 & ,S < -\varepsilon \end{cases} \quad (15)$$

B. Stability Analysis

Define a Lyapunov function candidate V, which is a positive definite function:

$$V = \frac{1}{2}S^TS + \frac{1}{2}tr\left(\tilde{K}_0^{\ T}\Gamma_1^{-1}\tilde{K}_0\right) + \frac{1}{2}tr\left(\tilde{B}_0^{\ T}\Gamma_2^{-1}\tilde{B}_0\right) + \frac{1}{2}tr(\tilde{C}_0^{\ T}\Gamma_3^{-1}\tilde{C}_0) + \frac{1}{2}tr(\tilde{W}_c^{\ T}\Gamma_4^{-1}\tilde{W}_c) \quad (16)$$

where $\Gamma_i = diag[\gamma_{i1}, \gamma_{i2}], i = 1\sim4,$ *a*re positive diagonal matrices, tr(.) is the trace of a matrix, and $\tilde{K}_0, \tilde{B}_0, \tilde{C}_0,$ and $\tilde{W}_0$ are the estimation errors, defined as $\tilde{K}_0 = \hat{K}_0 - K_0$, $\tilde{B}_0 = \hat{B}_0 - B_0$, $\tilde{C}_0 = \hat{C}_0 - C_0$, and $\tilde{W}_c = \hat{W}_c - W_c$. In the next step, by differentiating the Lyapunov function candidate, we obtain:

$$\dot{V} = S^T\dot{S} + tr\left(\tilde{K}_0^{\ T}\Gamma_1^{-1}\dot{\tilde{K}}_0\right) + tr\left(\tilde{B}_0^{\ T}\Gamma_2^{-1}\dot{\tilde{B}}_0\right) + tr(\tilde{C}_0^{\ T}\Gamma_3^{-1}\dot{\tilde{C}}_0) + tr(\tilde{W}_c^{\ T}\Gamma_4^{-1}\dot{\tilde{W}}_c) \quad (17)$$

Here, $\dot{S}$ can be calculated by Eq. (12) (13), and be reformulated by substituting U in Eq. (14):

$$\dot{S} = \tilde{C}_0U + \tilde{K}_0X + \tilde{B}_0\dot{X} + \tilde{W}_c + QS + Nsat(S) - W_v \quad (18)$$

so Eq. (17) becomes

$$\dot{V} = -S^T QS - S^T(Nsat(S) - W_v) + tr\left[\tilde{K}_0{}^T\left(\Gamma_1{}^{-1}\dot{\tilde{K}}_0 - SX^T\right)\right] + tr\left[\tilde{B}_0{}^T\left(\Gamma_2{}^{-1}\dot{\tilde{B}}_0 - S\dot{X}^T\right)\right] + tr\left[\tilde{C}_0{}^T\left(\Gamma_3{}^{-1}\dot{\tilde{C}}_0 - SU^T\right)\right] + tr\left[\widetilde{W}_c{}^T\left(\Gamma_4{}^{-1}\dot{\widetilde{W}}_c - S\right)\right] \quad (19)$$

By choosing the adaptive law of σ-modification [25], the boundedness in the presence of modeling error term can be determined in the following:

$$\dot{\hat{K}}_0 = \dot{\tilde{K}}_0 = \Gamma_1 S\dot{X} - \Gamma_1\Sigma_1\hat{K}_0,\ \dot{\hat{B}}_0 = \dot{\tilde{B}}_0 = \Gamma_2 SX - \Gamma_2\Sigma_2\hat{B}_0,$$
$$\dot{\hat{C}}_0 = \dot{\tilde{C}}_0 = \Gamma_3 SU - \Gamma_3\Sigma_3\hat{C}_0,\ \dot{\hat{W}}_c = \dot{\widetilde{W}}_c = \Gamma_4 S - \Gamma_4\Sigma_4\widehat{W}_c \quad (20)$$

where $\Sigma_1 = diag[\sigma_{i1}, \sigma_{i2}], i = 1\sim4$, are all positive diagonal matrices. By substitute Eq. (20) into Eq. (19), and choosing the large enough high gain N to dominant the time-varying uncertainty W_v, then we have

$$\dot{V} \le -S^T QS - S^T[Nsat(S) - W_v] - \sum_{i=1}^{2}\begin{Bmatrix}\frac{\sigma_{1i}}{2}[\|\tilde{k}_{0i}\|^2 - \|k_{0i}\|^2] + \frac{\sigma_{2i}}{2}[\|\tilde{b}_{0i}\|^2 - \|b_{0i}\|^2] \\ + \frac{\sigma_{3i}}{2}[\|\tilde{c}_{0i}\|^2 - \|c_{0i}\|^2 + \frac{\sigma_{4i}}{2}[\|\widetilde{w}_{ci}\|^2 - \|w_{ci}\|^2]\end{Bmatrix} \quad (21)$$

Choose $0 < \alpha < \min\begin{Bmatrix}2q_i, \gamma_{i1}, \sigma_{i2}, \gamma_{2i}, \sigma_{2i} \\ , \gamma_{3i}, \sigma_{3i}, \gamma_{4i}, \sigma_{4i}\end{Bmatrix},\ i = 1,2$, and add the term αV to Eq. (21), we can obtain the following inequality:

$$\dot{V} \le -S^T[Nsat(S) - W_v - W_S] - \alpha V + \sum_{i=1}^{2}\frac{1}{2}[\sigma_{1i}|k_{0i}|^2 + \sigma_{2i}|b_{0i}|^2 + \sigma_{3i}|c_{0i}|^2 + \sigma_{4i}|w_{ci}|^2] \quad (22)$$

Since sliding mode control scheme involving saturation function belongs to boundary layer control, the analysis of sliding parameter S inside or outside the boundary layer ε should be taken into consideration. After considering two situations in most conservative stability case, we apply Lyapunov stability theorem, $\dot{V} \le 0$ when

$$V \ge V_0 = \frac{1}{2\alpha}\sum_{i=1}^{2}\begin{bmatrix}\sigma_{1i}|k_{0i}|^2 + \sigma_{2i}|b_{0i}|^2 \\ +\sigma_{3i}|c_{0i}|^2 + \sigma_{4i}|w_{ci}|^2 + \frac{\varepsilon_i}{2\eta_i}\overline{W}^2\end{bmatrix} \quad (23)$$

implies that $V, \dot{V} \in L_\infty$and therefore $S, \dot{S}, E, \dot{E},\ \tilde{K}_0, \tilde{B}_0, \tilde{C}_0, \widetilde{W}_0 \in L_\infty$. Lastly, we can further show that $|E(t)|$ will converge to a residual set whose size is in the order of $\max\{\varepsilon_i,\ \sigma_{ij}\}$, which implies that such error performance can be improved by appropriate parameter choice.

V. Experimental Results

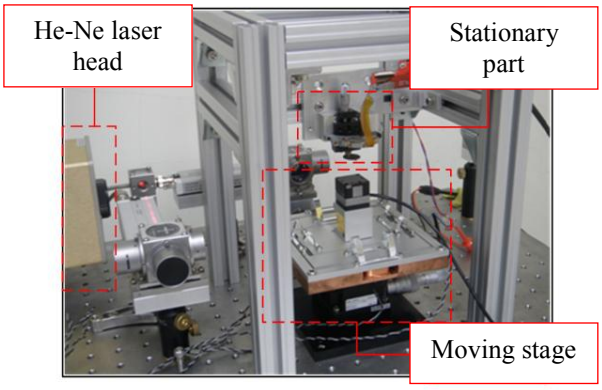

Fig. 6 The overall view of the AFM system

The overall AFM system, including the stationary part (scanning tools) and the moving stage (piezoelectric positioner and PEP), is shown in Fig. 6. In the stationary part, a CD/DVD PUH is fixed on the frame and the probe is mounted on the CD/DVD PUH's lens below. The distance between the probe and the stage is adjusted by a tuning linear stage. Under the probe, our measured sample lies on the designed moving stage which is driven by the adaptive sliding mode controller compiled in MATLAB Simulink. In the experiments, MATLAB xPC target is utilized for real-time control. Besides, Agilent N1231b A/D card is for laser interferometer sensing feedback, and NI 6733 D/A card with Copley Controls 412ce amplifiers are for output control signals. Due to the symmetric design and similar behavior, the following experiments in y-axis are omitted.

A. Step Response

To begin with, a 500 μm step signal was applied to the x-axis while y-axis was regulated to zero. Because C_0 in the controller can be considered as a constant, it was chosen to be 0.5 to simplify the computation. In Fig. 7 (a), we can see that the rise time is 0.15 sec, the settling time is 0.26 sec, the overshoot is 12%, and a steady state error of 28 nm in root-mean-square is calculated. Figure 7 (b) shows the regulation in y-axis, and the coupling displacement under the control effort is between ±3 μm. In Fig. 7 (c)-(e), the estimations of K_0, B_0, Wc are presented, where k_{ij}, b_{ij}, wc_i, i, j = 1,2, are the responding terms in K_0, B_0, Wc. As we can observe, the coupling terms in each matrix are not zero and all converge to arbitrary numbers.

B. Step Train

In our AFM scanning, each image frame is at least 8 μm². To realize the large scale scanning, a step train of 8 μm with a total distance of 40 μm was applied as shown in Fig. 8. Since the adaptive control is not strong enough for the transient state, some under-shoots and over-shoots are observed in such small scale; however, the good performance in the steady states with 30 nm rms error guarantees the positioning ability of PEP.

VI. Conclusion

In this paper, the design, implementation, and control of an AFM scanning instrument is presented. The compact design of PEP, consisting of a monolithic *xy* serial compliant flexure mechanism with compression spring, electromagnetic actuators, and an Eddy current damper is detailed. Moreover, a robust adaptive sliding mode controller, which is capable of dealing with the unmodeled parameters and external disturbances, is applied. In addition, a compact and low-cost CD/DVD PUH is applied. Utilizing this device we can actually reduce the complex light path and the sensing error. Finally, with the help of both piezoelectric and electromagnetic actuations, a large scale scanning is achievable, and some preliminary experiments have testified the positioning and AFM scanning abilities. To sum up, a large scale scanning AFM system has been proposed in this work. The integration of software between AFM scanning and PEP positioning is still under construction; more experiments are needed to identify the overall behavior of this instrument.

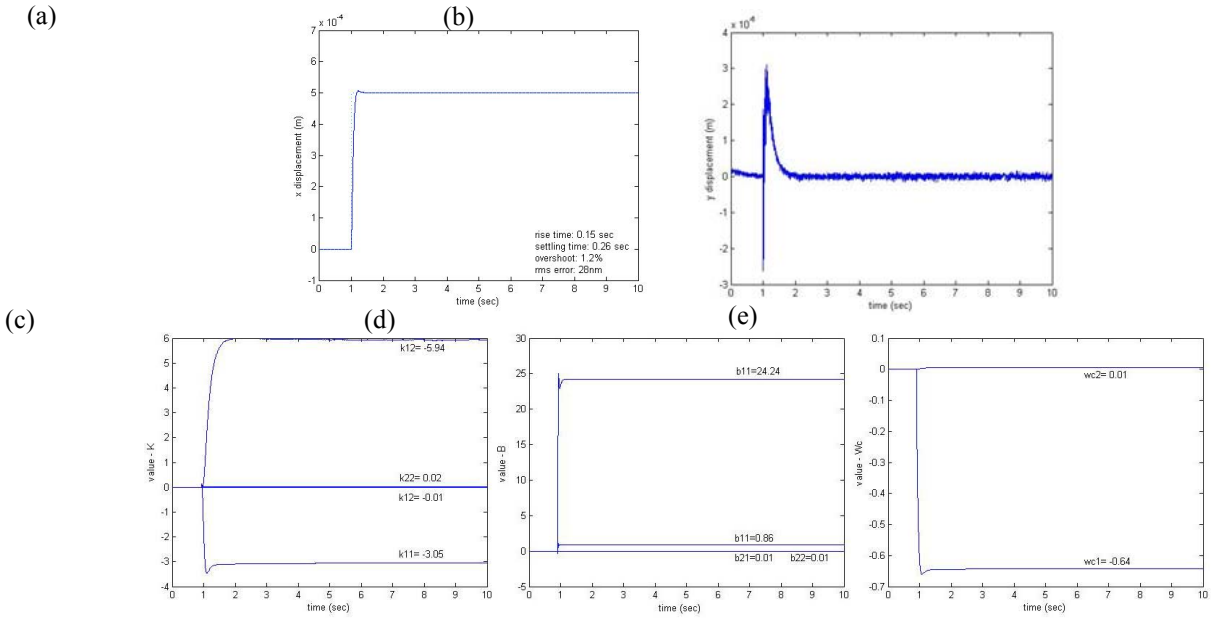

Fig. 7 Step response of 500 μm in *x*-axis at time t = 1 sec, while *y*-axis was regulated to zero. (a) the step response in *x*-axis (b) the regulation in *y*-axis (c) estimation of *K* (d) estimation of *B* (e) estimation of *Wc*

VII. REFERENCES

[1] G. Binning, C. F. Quate, and C. Gerber,"Atomic force microscope," Physical Review Letters, vol. 56, pp.930-933, 1986.

[2] Y. Martin, and H. K. Wickramasinghe, "Magnetic imaging by force microscopy with 1000 A resolution," Applied Physics Letters, 50:1455, 1987.

[3] C. M. Mate, G. M. McClelland, R. Erlandsson, and S. Chiang, "Atomic-scale frction of a tungsten tip on a graphite surface," Physical Review Letters, 59(17):1942-1945, 1987.

[4] Y. Martin, D. W. Abraham, and H. K. Wickramasinghe, "High-resolution capacitance measurement and potentiometry by force microscopy," Applied Physics Letters, 52:1103, 1988.

[5] D. Y. Abramovitch, S. B. Andersson, L. Y. Pao, and G. Schitter, "A tutorial on the mechanisms, dynamics, and control of atomic force microscopes," American Control Conference, pp. 3488–3502, 2007.

[6] I. Schmitz, M. Schreiner, G. Friedbacher, and M. Grasserbauer, "Phase imaging as an extension to tapping mode AFM for the identification of material properties on humidity-sensitive surfaces," Appl. Surface Sci., vol. 115, no. 2, pp. 190–198, Jun. 1997.

[7] A. Sinno, P. Ruaux, L. Chassagne, S. Topcu, Y. Alayli, G. Lerondel, S. Blaize, A. Bruyant, and P. Royer, "Enlarged atomic force microscopy scanning scope: Novel sample-holder device with millimeter range," REVIEW OF SCIENTIFIC INSTRUMENTS 78, 095107, 2007.

[8] A. Sinno, P. Ruaux, L. Chassagne, S. Topcu, Y. Alalyli, G. Lerondel, S. Blaize, A. Bruyant, P. Royer, "Enlarged Sample Holder For Optical Afm Imaging: Millimeter Scanning With High Resolution," IEEE, 2009.

[9] Brian J Eves, "Design of a large measurement-volume metrological atomic force microscope (AFM)," Meas. Sci. Technol. 20, 084003, 2009.

[10] C. Werner, P. C. J. N. Rosielle, M. Steinbuch, "Design of a long stroke translation stage for AFM," International Journal of Machine Tools & Manufacture 50, pp. 183–190, 2010.

[11] Won-jong Kim, Shobhit Verma, "Multiaxis Maglev Positioner With Nanometer Resolution Over Extended Travel Range," Journal of Dynamic Systems, Measurement, and Control, vol. 129, 2007

[12] Y. Liang, I. M. Chen, L. Chee Kian, Y. Guilin, L. Wei, and L. Kok-Meng, "Design and analysis of a permanent magnet spherical actuator," Mechatronics, IEEE/ASME Transactions on, vol. 13, no. 2, pp. 239–248, 2008.

[13] S. Hungsun and L. Kok-Meng, "Distributed multipole models for design and control of pm actuators and sensors," Mechatronics, IEEE/ASME Transactions on, vol. 13, no. 2, pp. 228–238, 2008.

[14] L. Petit, C. Prelle, E. Dore, F. Lamarque, and M. Bigerelle, "A fourdiscrete- position electromagnetic actuator: Modeling and experimentation," IEEE/ASME Transactions on Mechatronics, vol. 15, no. 1, pp. 88–96, 2010.

[15] J. Lei, X. Luo, X. Chen, and T. Yan, "Modeling and analysis of a 3-dof lorentz-force-driven planar motion stage for nanopositioning," Mechatronics, vol. 20, no. 5, pp. 553–565, 2010.

[16] M.-Y. Chen, H.-W. Tzeng, and S.-K. Hung, "A new mechanism design of electro-magnetic actuator for a micro-positioner," ISA Transactions, vol. 46, no. 1, pp. 41–48, 2007.

[17] S-K Hong, C-H Lin, M-Y Chen, S-T Li, and L-C Fu, "A Novel High Precision Electromagnetic Flexure-Suspended Positioning Stage with an Eddy Current Damper," Proc. International Conference on Control, Automation and Systems, pp. 771-776, 2008.

[18] Chih-Hsien Lin, Shao-Kung Hung, Sang-Tsung Li, and Li-Chen Fu,"High Precision Eddy Current Damped Electromagnetic Positioner with Flexure-Suspension," 18th IEEE International Conference on Control Applications, Part of 2009 IEEE Multi-conference on Systems and Control, Saint Petersburg, Russia, July 8-10, 2009

[19] Shan-Tsung Lee, Kuan-Lin Huang, Jim-Wei Wu, and Li-Chen Fu, "Design and Control of Long Travel Range Electromagnetically Actuated System with Application to Precise Machining," 2010 IEEE Multi-Conference on Systems and Control, September 8-10, 2010

[20] C. Mei-Yung, H. Hsuan-Han, and H. Shao-Kang, "A new design of a submicropositioner utilizing electromagnetic actuators and flexure mechanism," Industrial Electronics, IEEE Transactions on, vol. 57, no. 1, pp. 96–106, 2010.

[21] Kuan-Lin Huang, " Design and Implementation of a New Three-DOF Electromagnetically Actuated Precision Positioning Stage with Flexure Mechanism," Master Thesis, Grad. Institute of Electrical Engineering, College of Electrical Engineering and Computer Science, NTU, Taiwan, July, 2010

[22] Yuen Kuan Yong, Sumeet S. Aphale, and S. O. Reza Moheimani, Senior Member, IEEE "Design, Identification, and Control of a Flexure-Based XY Stage for Fast Nanoscale Positioning," IEEE Transactions on Nanotechnology, vol. 8, no. 1, January 2009

[23] Shih-Hsun Yen, Jim-Wei Wu, Li-Chen Fu, "Apply tapping mode Atomic Force Microscope with CD/DVD pickup head in fluid," American Control Conference (ACC), pp. 6549-6554, 2010.

[24] B. K. G. B.Bhushan, Hand book of tribology: McGraw-Hill, 1991.

[25] P. A. Ioannou, and J. Sun, Robust Adaptive Control, Prentice Hall, 1998